Atmos. Meas. Tech., 6, 3425–3440, 2013
www.atmos-meas-tech.net/6/3425/2013/
doi:10.5194/amt-6-3425-2013


Atmospheric Measurement Techniques
Open Access

# Reporting the sensitivity of laser-induced fluorescence instruments used for $HO_2$ detection to an interference from $RO_2$ radicals and introducing a novel approach that enables $HO_2$ and certain $RO_2$ types to be selectively measured

**L. K. Whalley[1,2], M. A. Blitz[1,2], M. Desservettaz[1], P. W. Seakins[1,2], and D. E. Heard[1,2]**

[1]School of Chemistry, University of Leeds, Leeds, LS2 9JT, UK
[2]National Centre for Atmospheric Science, University of Leeds, Leeds, LS2 9JT, UK

*Correspondence to:* L. K. Whalley (l.k.whalley@leeds.ac.uk)

Received: 11 June 2013 – Published in Atmos. Meas. Tech. Discuss.: 9 July 2013
Revised: 29 October 2013 – Accepted: 8 November 2013 – Published: 9 December 2013

**Abstract.** Laboratory studies have revealed that alkene-derived $RO_2$ and longer chain alkane-derived $RO_2$ ($> C_3$) radicals rapidly convert to $HO_2$ and then to OH in the presence of NO in a fluorescence assay by gas expansion (FAGE) detection cell (Fuchs et al., 2011). Three different FAGE cells that have been used to make ambient measurements of OH and $HO_2$ in the University of Leeds ground-based instrument have been assessed to determine the sensitivity of each cell, when operating in $HO_2$ detection mode, to $RO_2$ radicals. The sensitivity to this interference was found to be highly dependent on cell design and operating parameters. Under the operating conditions employed, during fieldwork undertaken in the Borneo rainforest in 2008, an OH yield of 17 % was experimentally determined for both ethene- and isoprene-derived $RO_2$ radicals. The high pumping capacity of this system, resulting in a short residence time in the cell, coupled with poor mixing of NO into the ambient air-stream for the titration of $HO_2$ to OH effectively minimised this potential interference. An OH yield of 46 % was observed for ethene-derived $RO_2$ radicals when a smaller detection cell was used, in which the mixing of NO into the ambient air was improved and the cell residence times were much longer. For a newly developed $RO_x$LIF cell, used for detection of $HO_2$ and $RO_2$ radicals an OH yield of 95 % was observed for ethene-derived $RO_2$ radicals, when running in $HO_2$ mode.

In experiments in which conditions ensured the conversion of $RO_2$ to OH were complete, the yields of OH from a range of different $RO_2$ species agreed well with model predictions based on the Master Chemical Mechanism version 3.2. For ethene and isoprene-derived $RO_2$ species, the relative sensitivity of FAGE was found to be close to that for $HO_2$, with an OH yield of 100 % and 92 %, respectively. For the longer chain or cyclic alkane-derived $RO_2$ radicals ($> C_3$), model predicted OH yields were highly dependent upon temperature. A model predicted OH yield of 74 % at 298 K and 36 % at 255 K were calculated for cyclohexane-derived $RO_2$ radicals, and an experimental yield of 38 % was observed indicating that the temperature within the cell was below ambient owing to the supersonic expansion of the airstream in the low pressure cell.

These findings suggest that observations of $HO_2$ by some LIF instruments worldwide may be higher than the true value if the instruments were sensitive to these $RO_2$ species. If this is the case, it becomes necessary to compare atmospheric chemistry model simulations to $HO_2^*$ observations, where $HO_2^* = [HO_2] + \Sigma_i \alpha_i [RO_2 i]$, and $\alpha_i$ is the mean fractional contribution of the $RO_2$ species that interfere ($RO_2 i$). This methodology, however, relies on model simulations of speciated $RO_2$ radicals, as instrumentation to make speciated $RO_2$ measurements does not currently exist. Here we present an approach that enables the concentration of $HO_2$ and $RO_2 i$ to be selectively determined by varying the concentration of NO injected into a FAGE cell. Measurements of $[HO_2]$ and $[RO_2 i]$ taken in London are presented.

**Published by Copernicus Publications on behalf of the European Geosciences Union.**

## 1 Introduction

OH and $HO_2$ radicals, collectively termed $HO_x$, together with $RO_2$ radicals, control the oxidative chemistry in the atmosphere, being responsible for the transformation of primary emissions into secondary pollutants such as $NO_2$, $O_3$ and particulates. OH radicals control the lifetime of some greenhouse gases (e.g. $CH_4$), the production of acidic species (e.g. $H_2SO_4$) and aerosol precursors such as oxygenated volatile organic compounds. Understanding the behaviour of free-radicals in the atmosphere is of paramount importance in understanding the lifetimes of pollutants and hence the spatial scales of their transport. Predictive models for future air quality and climate change contain complex chemical schemes, and comparison with measurements of free-radicals (the concentrations of which are controlled only by local chemistry and not by transport) in the present atmosphere constitutes one of the best validations of these schemes (Heard and Pilling, 2003). OH and $HO_2$ radicals in the troposphere have been measured since the early 1990s using laser-induced fluorescence (LIF) spectroscopy at low pressure (Fluorescence Assay by Gas Expansion, or the FAGE technique) originally developed by Hard et al. (1979, 1984). The technique employs 308 nm radiation, produced using a variety of laser technologies, to excite OH radicals, which fluoresce; this emission (also at 308 nm) is detected and used to quantify OH. It is also possible to simultaneously detect $HO_2$ in a second fluorescence cell, by chemical conversion to OH through reaction with NO and subsequent detection by LIF. The technique has been employed by several groups worldwide for the detection of OH and $HO_2$ (Hofzumahaus et al., 1996; Mather et al., 1997; Kanaya et al., 1999; Creasey et al., 2001; Faloona et al., 2001; Hanisco et al., 2002; Holland et al., 2003; Heard and Pilling, 2003; Stone et al., 2012). Specific to this work, the Leeds ground-based FAGE instrument has been operational since 1996 and has detected OH and $HO_2$ under a variety of conditions ranging from urban (Heard et al., 2004) to clean marine (Whalley et al., 2010). Although the FAGE technique represents an extremely sensitive (typical OH detection limits are in the low to mid- $10^5$ molecule $cm^{-3}$) (Heard and Pilling, 2003) and selective method for OH and $HO_2$ detection, ambient $HO_x$ concentrations are themselves extremely low (OH concentrations are typically a few $10^6$ molecule $cm^{-3}$) (Stone et al., 2012), thus, care needs to be taken to ensure that any measurement is not biased by any chemical or spectral interference.

A well-documented example of an OH interference comes from the earliest tropospheric LIF instruments (Davis et al., 1981; Ortgies et al., 1980; Shirinzadeh et al., 1987), which used off-resonant pulsed laser excitation of the OH radical at 282 nm, via the $A^2\Sigma^+(\upsilon' = 1) \leftarrow X^2\Pi_i(\upsilon'' = 0)$ transition. These instruments were found to suffer from a considerable interference from laser-generated OH formed by the laser photolysis of ambient ozone and subsequent reaction of $O(^1D)$ with ambient water vapour:

$$O_3 \xrightarrow{hv} O(^1D) + O_2 \quad \text{(R1)}$$

$$O(^1D) + H_2O \rightarrow 2OH \quad \text{(R2)}$$

The use of OH detection at lower pressure (reducing $[H_2O]$ and hence the rate of Reaction R2), lower laser energy per pulse (the OH artefact signal depends on the square of the laser energy) and switching to excitation at 308 nm (the $H_2O/O_3$ interference is 30 times lower than at 282 nm) almost completely overcame this problem. Holland et al. (2003), however, observed an interference in the presence of ozone and water vapour that appeared to be a dark reaction on the walls of their detection cell which produced a source of $HO_2$ radicals; the authors report a signal equivalent to $5.4 \times 10^7$ molecule $cm^{-3}$ of $HO_2$ in the presence of 50 ppbv $O_3$ and at a relative humidity of 60 %. This interference has been characterised in detail and is subtracted from their ambient $HO_2$ measurements.

In the presence of the added NO used to convert $HO_2$ to OH inside the fluorescence cell, and hence enable $HO_2$ to be measured, organic peroxy radicals ($RO_2$) also have the potential to be chemically converted to OH via:

$$RO_2 + NO \rightarrow RO + NO_2 \quad \text{(R3)}$$

$$RO + O_2 \rightarrow HO_2 + R_{-H}O \quad \text{(R4)}$$

$$HO_2 + NO \rightarrow OH + NO_2 \quad \text{(R5)}$$

Due to the low pressure employed in FAGE detection, however, Reaction (R4) is slow ($\sim 12\,s^{-1}$ for $CH_3O$ at 1 Torr) and, given the very short residence time in FAGE between NO injection and the detection region of typically just a few milliseconds or less (Creasey et al., 1997b), it was assumed, until recently, that $RO_2$ radicals were not converted to OH to any large extent. In support of this, Ren et al. (2004) reported no interference upon introduction of $C_1$–$C_4$ alkane-derived $RO_2$ radicals in the Penn State FAGE system, and concluded that there was no evidence of any significant interferences for OH or $HO_2$ measurements in the atmosphere, including in highly polluted urban environments. Only recently has an interference from alkene and aromatic-derived $RO_2$ species been reported (Fuchs et al., 2011). Unlike alkane-derived $RO_2$ species which are formed via H-atom abstraction from the parent alkane and subsequent addition of $O_2$ (Reaction R6), the major pathway to alkene-derived $RO_2$ formation is via OH addition across the double bond followed by $O_2$ addition (Reaction R7):

$$RH + OH \xrightarrow{O_2} RO_2 + H_2O \quad \text{(R6)}$$

$$R = R' + OH \xrightarrow{O_2} R(OH) - R'O_2 \quad \text{(R7)}$$

$$R(OH) - R'O_2 + NO \rightarrow R(OH) - R'O + NO_2 \quad \text{(R8)}$$

$$R(OH) - R'O + O_2 \rightarrow R(OH) - R'_{-H}O + HO_2 \quad \text{(R9)}$$

$$R(OH) - R'O \xrightarrow{\text{Decomp.}} R = O + R' - OH \quad \text{(R10)}$$

$$R' - OH + O_2 \rightarrow R = O + HO_2 \quad \text{(R11)}$$

The $\beta$-hydroxyalkylperoxy radical formed reacts with NO to form the $\beta$-hydroxyalkoxy radical Reaction (R8) which can either react with $O_2$ (Reaction R9) or decompose to a hydroxyalkyl radical (Reaction R10) which then reacts rapidly with $O_2$ to form a carbonyl and $HO_2$ (Reaction R11). Compared to the slow $RO + O_2$ reaction ($k = 1.65 \times 10^{-15}$ cm$^3$ molecule$^{-1}$ s$^{-1}$, for R = $CH_3$, Reaction R9; Orlando et al., 2003), decomposition and subsequent reaction of the hydroxyalkyl radical ($CH_2OH$) with $O_2$ is fast ($k = 9.6 \times 10^{-12}$ cm$^3$ molecule$^{-1}$ s$^{-1}$; Atkinson et al., 1997). Fuchs et al. (2011) found, due to this rapid decomposition pathway, that $RO_2$ species formed from alkene and aromatic precursors were detected as OH with relative sensitivities greater than 80 % with respect to that for detection of $HO_2$ in their FAGE system. The level of the interference was found to be highly dependent upon the NO concentration injected and reaction time between injection and OH detection, which was varied by Fuchs et al. (2011) suggesting that other FAGE instruments with different cell designs and operational parameters may display different sensitivities towards this interference. FAGE cells used for airborne $HO_2$ measurements tend to have longer inlets to extend through the fuselage of the aircraft and, hence, sampled air tends to have longer residence times in these cell types compared to cells used solely for ground measurements. Very recently, Mao et al. (2012) reported an average $RO_2$ sensitivity of $\sim$ 60 % with respect to that for $HO_2$ for a selection of alkene-derived $RO_2$ species in the Penn State FAGE instrument, whilst Vaughan et al. (2012) reported a sensitivity to ethene-derived $RO_2$ radicals of 40 % with respect to that for $HO_2$ for the University of Leeds aircraft FAGE instrument (Commane et al., 2010). Ultimately, the measurement bias on the $HO_2$ concentrations reported from past field studies will depend upon the individual FAGE instruments utilised (because of variations in key operating parameters such as residence time) and the concentration and speciation of $RO_2$ present. Many FAGE groups now report $HO_2^*$ for comparison with atmospheric chemistry box models (Lu et al., 2012) where $HO_2^* = [HO_2] + \Sigma_i \alpha_i [RO_2 i]$, and $\alpha_i$ is the mean fractional contribution of the $RO_2$ species that interfere ($RO_2 i$) in a particular instrument which has been determined experimentally.

Together with a $HO_2$ interference, FAGE measurements of OH are reported to have an interference for one instrument type in forested environments (Mao et al., 2012). The authors postulate that OH may be generated in their FAGE cell in the presence of ozone and alkenes, with laser-generated OH within the cell being ruled out. Similar to the $HO_2$ interference reported here, this OH interference may be dependent upon the particular design of this FAGE cell, for example the residence time between sampling and detection and, as such, the extent that other OH measurements suffer from this interference is unknown, meaning that it is critical that a set of standardised experiments are performed on different FAGE cell types used for ambient detection of OH to assess the extent of any interference. Good agreement between two independent OH measurements made using Differential Optical Absorption Spectroscopy (DOAS) and LIF was observed during a series of experiments performed in the SAPHIR atmospheric simulation chamber under a range of atmospheric conditions (Fuchs et al., 2012, 2013) suggesting that the Julich FAGE system, at least, does not suffer an interference when detecting OH under the conditions studied.

In this paper we report results from interference studies performed using the University of Leeds ground-based FAGE instrument (Creasey et al., 1997a) measuring in $HO_2$ mode (NO added to the detection cell) and discuss the likely impact of the $RO_2$ interference on previous field studies. We also compare absolute yields of OH from alkene-derived and higher alkane-derived $RO_2$ species in the presence of NO with MCMv3.2 recommendations, where experimental conditions allowed reactions to proceed to completion.

## 2 Experimental

$HO_2$ and $RO_2$ radicals were generated prior to FAGE detection by two different methods: a steady-state turbulent flow tube reactor calibrated for absolute radical concentrations and a time-resolved laser flash photolysis system. Each method will be described in turn.

### 2.1 Steady-state experiments

The FAGE calibration system (described in detail by Commane et al., 2010) acts as a turbulent flow reactor and generates known and equal quantities of OH and $HO_2$ radicals by the 184.9 nm photolysis of $H_2O$ vapour by a Hg penray lamp in a humidified air stream (Reactions R12–13):

$$H_2O + h\nu \rightarrow H + OH \quad \text{(R12)}$$

$$H + O_2 \xrightarrow{M} HO_2 \quad \text{(R13)}$$

With knowledge of the product of the lamp flux and irradiation exposure time past the lamp (determined by $N_2O$ actinometry; Commane et al., 2010), the concentration of OH and $HO_2$ may be determined; typical radical concentrations generated by this method range from $< 10^7$–$10^9$ molecule cm$^{-3}$. $RO_2$ radicals (in the presence of $HO_2$

from Reaction R13) were generated by introducing the parent hydrocarbon into the FAGE calibration system approximately 2.5 cm after the penray lamp. The OH generated in the calibration photolysis region reacted rapidly with the hydrocarbon introduced, Reactions (R6) or (R7), generating $RO_2$ radicals. To assess the magnitude of any $HO_2$ interference suffered during previous ambient field measurements, a number of individual peroxy radical species were generated and introduced into three different fluorescence cells (Fig. 1) which have been used during field deployments by the Leeds group (further details on the fieldwork FAGE detection cells tested are given below). The peroxy radicals tested were derived from methane, propane, ethene, isoprene, toluene, cyclohexane and methanol. A small flow ($\sim$ 10–150 standard cubic centimetre per minute, SCCM) of a dilute (0.1–5 %) hydrocarbon mix in $N_2$ (ethene, isoprene, toluene, cyclohexane or methanol) or a 100 % hydrocarbon flow of propane (10 SCCM) or methane (500 SCCM) was introduced into a 20–40 standard litre per minute (SLM) humidified air-stream approximately 5 cm before the exit of the calibration tube. The residence time within the calibration flow tube ($\sim$ 10 ms at 40 SLM) was sufficient to ensure complete conversion of OH to $RO_2$ before being sampled in the fluorescence cells. In the case of ethene, at an initial concentration of $3.1 \times 10^{14}$ molecule cm$^{-3}$, it takes $\sim$ 1 ms for complete conversion of OH to $RO_2$, using a rate coefficient ($k_{C_2H_4+OH}$) equal to $2.86 \times 10^{-11}$ molecule$^{-1}$ cm$^3$ s$^{-1}$ (Cleary et al., 2006). This could be experimentally verified by observing the complete loss of the OH signal upon addition of the hydrocarbons when no NO was added to the FAGE expansion cells; this complete loss of OH signal was observed even for the slowest reacting hydrocarbon species, methane.

## FAGE detection cells

The University of Leeds ground-based FAGE instrument described in detail elsewhere (Whalley et al., 2010) was assessed to determine the magnitude of the $HO_2$ interference from selected $RO_2$ species under configurations employed in two recent field studies. The first, the Oxidants and Particle Photochemical Processes (OP3) (Hewitt et al., 2010) which took place in the Borneo rainforest (Whalley et al., 2011) and the second, the Hill Cap Cloud Thuringer – 2010 (HCCT-2010) which aimed to quantify the loss of radicals to cloud droplets.

The operational parameters of the different FAGE fluorescence cells considered are quite different and are summarised in Table 1. During OP3, one 22 cm internal diameter cylindrical, stainless steel fluorescence cell (cell A) was used to make sequential measurements of OH and $HO_2$ (Fig. 1a). Air was drawn into the cell via a 5 cm tall, 2.54 cm diameter turret through a 1 mm diameter pinhole nozzle in a flat plate (0.1 mm thickness). The cell was maintained at approximately 0.9 Torr using a Roots blower backed by

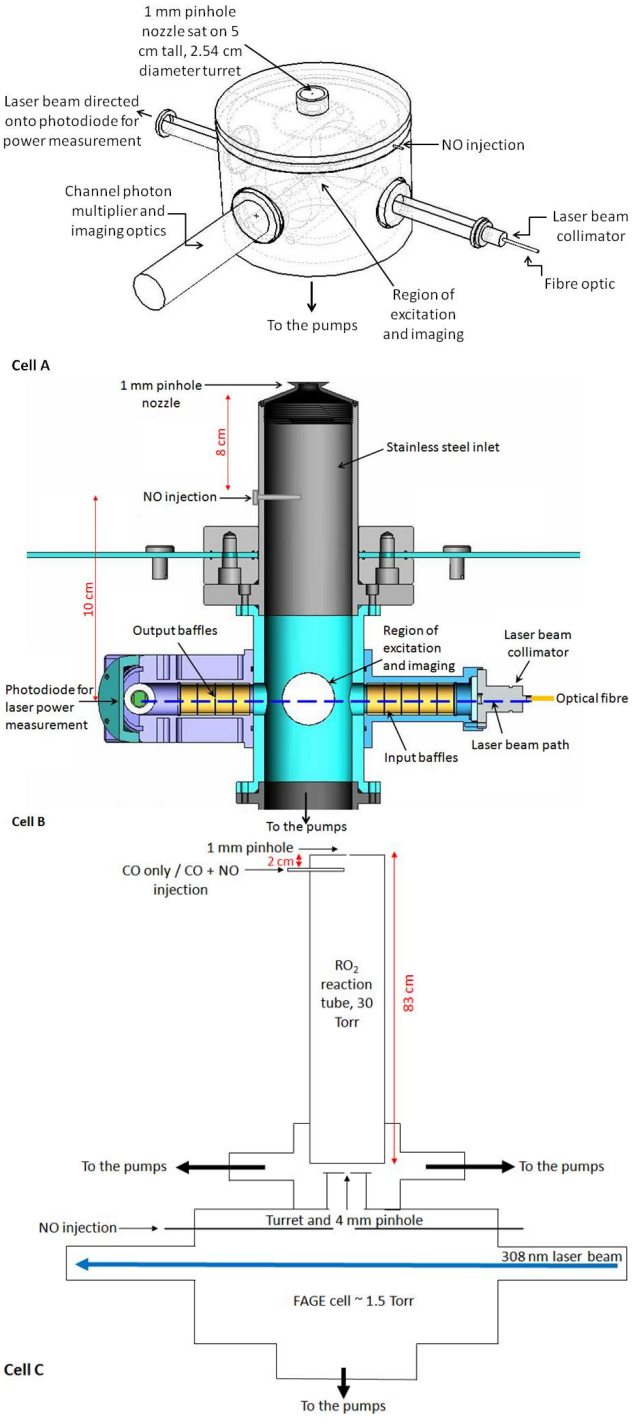


**Fig. 1.** Schematics highlighting the key features of the three FAGE cells tested. Cell A was used for sequential OH and $HO_2$ detection during the OP3 project; dotted line highlights internal cell components. Cell B was used to make sequential tower-based measurements of OH and $HO_2$ during the HCCT campaign. Cell C represents the coupling of a reaction tube to a FAGE cell (cell A design) for detection of $RO_2$ radicals by LIF, see text for further details.

a rotary pump (Leybold). The cell was connected to the pump system via a 10 cm ID, 5 m length stainless steel flexible hose. NO was injected into the cell 7.5 cm below the nozzle via a custom-built injection ring containing four injection points, spaced 4 cm apart, and made from 1.6 mm (ID) tubing in a square arrangement located around the air stream. In all, 50 SCCM NO was injected into the cell via a computer-controlled solenoid valve (Metron Semiconductors) and calibrated mass flow controller (MKS 1179A, range 0–50 SCCM) during the second half of the collection period when the laser was tuned to the OH transition. As only one cell was used for sequential detection of OH and $HO_2$, the conditions were optimised to maximise the sensitivity towards OH. Under these conditions the conversion of $HO_2$ to OH was only $\sim 10$ %, most likely due to poor mixing of the NO into the ambient air flow caused by the particular flow characteristics created by the combination of the 1 mm diameter pinhole nozzle and the pressure and pumping speeds employed. The 10 % conversion of $HO_2$ to OH determined assumes that there is no preferential loss of either radical in the calibration system (i.e. that the concentration of OH and $HO_2$ are equal as they enter the FAGE detection cell). This assumption has previously been verified by the addition of sufficient CO to the calibration system so as to rapidly convert all the OH to $HO_2$ (Reaction R14) and the $HO_2$ signal was observed to double in the presence of CO. The radicals sampled, or converted from $HO_2$, were electronically excited at 308 nm, approximately 13 cm below the sampling nozzle using a tuneable, 5 KHz pulse repetition frequency laser (Nd : YAG pumped Ti : Sapphire, Photonics Industries) with the fluorescence at the same wavelength detected perpendicular to the laser axis by a filtered (Barr Associates filter, transmission > 50 % at 308 nm) channel photo-multiplier (CPM, Perkin Elmer) and gated-photon counting.

During the HCCT-2010 campaign a single FAGE fluorescence cell was used to measure both radical species (cell B). The cell was operated from the top of a 22 m high tower to co-locate with hill-cap cloud measurements and ensure that the radical measurements were performed in full cloud when it had formed. As a result of these requirements a smaller cell, based on the University of Leeds aircraft FAGE fluorescence cell (Commane et al., 2010), was used to make sequential measurements of OH and $HO_2$ (Fig. 1b); operational details are provided in Table 1. NO (10 SCCM) was injected into this cell via 3.2 mm ID stainless tubing inserted into the centre of the ambient air stream. This configuration resulted in a high conversion of $HO_2$ to OH ($\sim 90$ %). Ambient air was drawn into the cell through a 1 mm diameter pinhole nozzle into a 4.5 cm (ID) stainless steel cylinder. The cell was held at 1 Torr and was connected to the roots-rotary pump system, described above, via 30 m of flexible hosing (5 cm ID). Laser light was delivered from the Nd : YAG pumped Ti : Sapphire laser system to the cell via a 30 m fibre optic. The distance between sampling nozzle and detection was 18 cm with the NO injected $\sim 8$ cm below the nozzle.

The third FAGE cell (cell C) tested for an $RO_2$ interference was a recently developed fluorescence cell designed for the detection of $RO_2$ radicals, alongside OH and $HO_2$, using the "$RO_x$LIF" methodology outlined by Fuchs et al. (2008). The $RO_2$ cell is operated in two modes, providing a measurement of the sum of OH + $HO_2$ in $HO_x$ mode and the sum of OH + $HO_2$ + $RO_2$ in $RO_x$ mode. Experiments were run on this third FAGE cell to determine the magnitude of the $HO_2$ interference suffered from a variety of $RO_2$ species in the $HO_x$ mode.

A similar FAGE fluorescence cell as the one described above (Fig. 1a, cell A) was modified by coupling it to a differentially pumped reaction tube (held at approximately 30 Torr) to allow for conversion of $RO_2$ radicals to OH (Fig. 1c). The reaction tube is an 83 cm high, 6.4 cm diameter aluminium tube which has been coated with halocarbon wax to minimise radical wall losses. Ambient air (7.5 SLM) is drawn into the reaction tube through a 1 mm diameter pinhole drilled into a thin (1 mm thickness), flat plate aluminium inlet nozzle. In $HO_x$ mode, 250 SCCM of CO (5 % in $N_2$, BOC) is flowed into the centre of the reaction tube just beneath the inlet ($\sim 2$ cm below) via a 6.4 mm (ID) stainless steel tube. Hydroxyl radicals are converted to $HO_2$ by reaction with CO (Reaction R14) as they pass through the reaction tube. Air ($\sim 5$ SLM) from the reaction tube is sampled by the FAGE detection cell (held at approximately 1.5 Torr) via a 4 mm diameter pinhole nozzle set on a 5 cm tall turret. Ambient $HO_2$ (and ambient OH which was converted to $HO_2$ in the reaction tube) is titrated to OH by NO injected into the cell 7.5 cm below the nozzle and detected by LIF; 100 SCCM of NO was injected into this fluorescence cell to maximise the conversion of $HO_2$ to OH. In $RO_x$ mode, 25 SCCM of a 500 ppmv NO standard in $N_2$ (BOC) was added to the CO flow to promote conversion of $RO_2$ to OH (Reactions R3–R5); the excess CO present rapidly converts OH to $HO_2$ (Reaction R14) and helps to minimise the overall loss of the radicals to the walls of the reaction tube. Ambient $RO_2$, $HO_2$ and OH radicals (converted to $HO_2$ in the reaction tube) enter the FAGE detection cell, are reconverted to OH by NO and detected as described above.

$$OH + CO \xrightarrow{O_2} HO_2 + CO_2 \quad \text{(R14)}$$

### 2.2 Time-resolved experiments using laser flash photolysis

The time-resolved set-up was based on a laser-induced pump and probe OH reactivity technique developed by Sadanaga et al. (2004) which uses pulsed 266 nm light to photolyse ozone in a flow tube to generate $O(^1D)$ and, by the subsequent reaction of $O(^1D)$ with $H_2O$ vapour, OH radicals (Reactions R1–R2). The flow tube used here was 173 cm in length with an internal diameter of 5 cm; a schematic of the experimental set-up is shown in Fig. 2. The total flow was typically 11 SLM and the pressure in the flow tube was 300 Torr, which was controlled by a valve throttling a rotary pump (Leybold). It

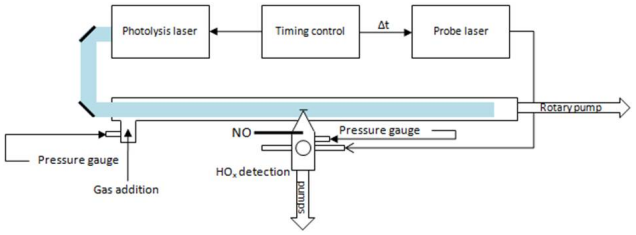


**Fig. 2.** Schematic highlighting the key features of the laser flash-photolysis time-resolved experimental set-up.

should be noted that at the pressures employed in the experiments, the high pressure limit of any pressure-dependent reactions taking place in the flow tube will have been reached and the results presented will be applicable to atmospheric conditions. A FAGE cell was located approximately halfway along the flow tube, held perpendicular to the flow tube, and sampled the gas flow through a 1 mm diameter pinhole nozzle that was located within 1 cm of the central axis of the flow tube. At the flow rates and pressure employed, the residence time in the flow tube before sampling was $\sim 4$ s. A YAG laser (Spectron SL803) was used to generate $\sim 10\,\mathrm{mJ\,pulse^{-1}}$ of 266 nm photolysis radiation with a 10 ns pulse width. The laser beam profile was shaped using a Galilean telescope to produce a collimated beam with a diameter of $\sim 2$ cm and directed along the flow tube such that the outer edge just illuminated the pinhole – gauged by the silhouette of the beam profile at the end of the tube.

The FAGE expansion cell was pumped by a rotary/Roots blower pump combination (Leybold), which reduced the pressure in the expansion cell to 1 Torr, and typically sampled about 30 % of the total flow of the flow tube with the remaining flow evacuated from the flow tube via the rotary pump. The expansion cell was 4.5 cm in internal diameter with the fluorescence detection axis $\sim 23.5$ cm from the pinhole. An excimer (Lambda Physik LPX105) pumped dye laser (Lambda Physik FL3002) operating on Rhodamine 6G generated visible light which was frequency doubled to 307.844 nm and used to probe the OH radical via the $Q_1$ (1) ($A$-$X$) (0-0) transition; typical pulse energies and pulse lengths were $0.2\,\mathrm{mJ\,pulse^{-1}}$ and 20 ns respectively. The radiation was directed into the detection axis via a baffled entrance arm and the fluorescence was captured by a filtered (Barr Associates), gated CPM (Perkin Elmer) mounted at right-angles to the laser beam. The pump and probe lasers were typically operated with a pulse repetition frequency of 2.5 Hz.

A LabView™ program controlled the experiment via a GPIB interfaced to a delay generator (Berkley Nucleonics Corporation, BNC 555) and an oscilloscope (LeCroy LT264). The time between the photolysis and probe lasers was controlled by the delay generator, and OH time profiles were built-up by scanning the delay between the lasers over 200 points. At each time point the OH fluorescence signal was integrated across its entire decay on the oscilloscope before being transferred for storage on the computer.

Gases were introduced to the flow tube via calibrated mass flow controllers (MKS). Nitrogen (10 SLM), was passed through a water bubbler (HPLC grade) and then into a manifold to mix with oxygen (1 SLM), ozone ($\leq 10$ standard cubic centimetres – SCCM) and a reagent gas ($\leq 40$ SCCM), before admission into the flow tube. Although the $O_2$ mixing ratio of the total flow was only $\sim 0.1$, this was sufficient to drive completely $RO_2$ formation in the flow tube (and OH formation within the FAGE cell in the presence of NO), and so behaves in the same way as an $O_2$ fraction of 0.2. Ozone from an ozone generator (Easelec, ELO-3G) was used directly to fill a 5 L Pyrex bulb, and then pressurised with nitrogen (up to 2 bar) to give concentrations between 1–3 %. The reagent gases, methanol, *n* butane, *n* pentane, ethene, isoprene and cyclohexane were degassed by freeze pump thawing, and known concentrations were prepared in Pyrex 5 L bulbs. Pressure gauges (MKS) were used to determine the bulb concentrations and the pressure in the flow tube and FAGE cell.

The OH generated (approximately $10^{10}\,\mathrm{molecule\,cm^{-3}}$) via the photolysis of ozone in the presence of $H_2O$ vapour (Reactions R1–R2) reacted rapidly with the added reagents (at a rate of $>1000\,\mathrm{s^{-1}}$) in the presence of $O_2$ forming peroxy radicals (Reactions R6 or R7) or in the case of methanol, $HO_2$ formed via the following reactions:

$$\mathrm{OH + CH_3OH \rightarrow CH_2OH + H_2O} \quad \text{(R15)}$$

$$\mathrm{CH_2OH + O_2 \rightarrow HO_2 + CH_2O} \quad \text{(R16)}$$

or

$$\mathrm{OH + CH_3OH \rightarrow CH_3O + H_2O} \quad \text{(R17)}$$

$$\mathrm{CH_3O + O_2 \rightarrow HO_2 + CH_2O} \quad \text{(R18)}$$

OH reacts with methanol, predominantly forming $CH_2OH$ (reported yields of 0.75–0.85; Atkinson et al., 2004) (Reaction R15) which then rapidly reacts with $O_2$ ($9.6 \times 10^{-12}\,\mathrm{cm^3\,molecule^{-1}\,s^{-1}}$) (Atkinson et al., 2004) to form $HO_2$ (Reaction R16). The other, minor, abstraction channel produces $CH_3O$, which reacts slower with $O_2$ ($1.92 \times 10^{-15}\,\mathrm{cm^3\,molecule^{-1}\,s^{-1}}$) (Atkinson et al., 2004) to produce $HO_2$ (Reactions R17 and R18). $HO_2$ generated in the system was detected by adding nitric oxide (NO-99.95 %, BOC) to the FAGE expansion cell (Fig. 2) to titrate to OH for subsequent detection (Reaction R5). The NO flow, controlled by a mass flow controller (Brookes) (0–50 SCCM), was injected into the centre of the FAGE cell, via 3.2 mm stainless steel tubing, approximately 13.75 cm below the pinhole. The fluorescence signal observed when NO was added to the expansion cell derived from OH and converted $HO_2$ ($\mathrm{OH} + \alpha\,\mathrm{HO_2}$), where $\alpha$ is equal to the titration efficiency

of Reaction (R5), which is a function of the amount of NO added and the contact time in the expansion cell. For complete conversion of $HO_2$ to OH in the detection cell $\alpha$ will equal 1. If this is the case, in the presence and absence of methanol there should be no overall change in the initial fluorescence signal when NO was added as the OH lost in Reaction (R15) is rapidly converted to $HO_2$ in Reaction (R16) and then back to OH via reaction with NO. In the time-resolved experiments, a 6 SCCM flow of NO was found to provide the maximum conversion of $HO_2$ to OH (close to 100 %).

### 2.3 Model comparison

The measured $HO_2$ yields from the different $RO_2$ species studied have been compared with model predictions based on the Master Chemical Mechanism (MCM) version 3.2 (http://mcm.leeds.ac.uk/MCM/home.htt) (Jenkin et al., 1997, 2003; Carslaw et al., 1999b; Saunders et al., 2003; Bloss et al., 2005). The chemical reactions which convert the various VOC tested to OH that were incorporated in the model are listed explicitly in the Supplementary information (SI). The MCM makes the assumption that alkoxy radicals either react with $O_2$ to form a carbonyl species and $HO_2$ or decompose (or in the case of the $>C_3$ alkane-derived alkoxy radicals, isomerise) to form a hydroxyalkyl radical. Within a low temperature FAGE expansion, however, in the presence of NO, the reaction of alkoxy radicals and NO may begin to compete as the rate of decomposition and isomerisation slows considerably at reduced temperatures (as discussed further in Sect. 4, temperatures may drop as low as 25 K within the jet and remain below ambient temperatures in the region between NO injection and detection; Creasey et al., 1997b). To account for this, Reaction (R19) has been included in model predictions with all rate coefficients for the reaction of various RO radicals with NO taken from the review paper by Heicklen (2007).

$$RO + NO \xrightarrow{M} RONO \quad \text{(R19)}$$

For reactions between alkoxy radicals and NO which do not have reported rate coefficients, $k_{RO+NO} = 3.3 \times 10^{-11}$ cm$^3$ molecule$^{-1}$ s$^{-1}$, (average rate coefficient for reaction of $C_3$ – $C_5$ RO radicals with NO) was assumed. The model was initialised with the radical concentrations used and [NO] and [$O_2$] which encompassed experimental conditions within the FAGE expansion cell. The concentrations of all other intermediate species or products were initialised as zero. [NO] was varied between $1 \times 10^{13}$–$1 \times 10^{15}$ molecule cm$^{-3}$ depending upon the NO flow rates introduced to each of the FAGE detection cells. For the large FAGE detection cell (of the style cell A), good agreement between the model and experiment is only achieved if the concentration of NO in the jet is lower than that calculated from the initial NO injection flow rate suggesting that the mixing within the jet is poor for this cell (see Sect. 4.2 for further details). The simultaneous rate equations were solved using an Excel based integrator, Kintecus (Ianni, 2002). The model runs were 80 ms in duration, which provided sufficient time for complete conversion of peroxy radicals to OH under the time-resolved experimental conditions discussed above.

## 3 Results

### 3.1 $RO_2$ interferences in $HO_2$ measurements using fieldwork FAGE instrumentation

A variety of $RO_2$ species were generated in the turbulent flow reactor and introduced into the three FAGE cells, A–C (Fig. 1) described in Sect. 2.1.1. The yield of OH from the different $RO_2$ species for the different cells is given in Table 1. The flow reactor produces OH and $HO_2$ in equal quantities in the absence of a hydrocarbon (Fuchs et al., 2011). Upon addition of a hydrocarbon all the OH generated is quickly consumed (on a timescale of the order of 1 m s$^{-1}$) and $RO_2$ radicals form. In the case of propane or methane, the $RO_2$ formed does not yield appreciable OH (via the formation of $HO_2$) in the FAGE expansion cells in the presence of NO (as shown by the time-resolved experiments, Sect. 3.2, the OH yield from propane was < 4 %), and so any fluorescence signal observed upon NO addition relates solely to the co-generated $HO_2$. The yield of OH from $RO_2i$ species can be determined by comparing the fluorescence signal observed when a $RO_2i$ species was present ($HO_x$ signal$_{(reagent)}$) with the OH yield from $HO_2$ alone ($HO_2$ signal in the propane or methane experiments, which have no interference) using Eq. (1):

$$\text{Relative OH yield} = \frac{HO_x \text{ signal}_{(reagent)} - HO_2 \text{signal}}{HO_2 \text{ signal}}. \quad (1)$$

The flows of hydrocarbons were adjusted so that equivalent OH reactivities ($k_{HC+OH}$ [HC]) for each of the hydrocarbons tested were used to ensure that any other loss of OH in the turbulent flow reactor (e.g. loss to walls) did not bias the relative yields determined.

In a number of experiments the NO concentration added to detection cell A was varied and the ratio of the OH signal observed for propane-derived $RO_2$ radicals relative to ethene-derived $RO_2$ radicals were compared and are shown in Table 1 and Fig. 4. As the NO concentration was reduced the interference from alkene-derived $RO_2$ radicals decreased. By varying [NO], it becomes possible to discriminate ambient $RO_2$ radicals from ambient $HO_2$ radicals and this is discussed further in Sect. 4.2.

### 3.2 Time-resolved experiments

To determine the absolute yield of OH from different $RO_2$ radicals in the presence of NO, a range of $RO_2$ radicals (or $HO_2$ in the case of methanol) were generated by the addition of different parent hydrocarbons to the flow tube described in Sect. 2.2 coupled to a FAGE cell in which there

**Table 1.** Experimentally determined OH yields (derived using Eq. 1) from peroxy radicals ($RO_2 \rightarrow HO_2 \rightarrow OH$) in continuous flow experiments for FAGE cells operated under fieldwork conditions and comparison with the MCMv3.2 OH yield. The modelled OH yield was determined using Eq. (4).

| Source of peroxy radicals | Flow of NO (SCCM) | Cell A, OH yield – Residence time: ~0.9 ms[a] – Typical NO flow used during fieldwork: 50 SCCM[b] – Flow rate through pinhole: 4.8 SLM – Cell Pressure: 0.9 Torr | MCM OH yield (referenced to initial $[RO_2]$) assuming a reaction time of 0.9 ms, a temperature of 255 K and $[NO] = 1 \times 10^{14}$ molecule cm$^{-3}$ | Cell B, OH yield – Residence time: ~1.9 ms[c] – Typical NO flow used during fieldwork: 10 SCCM – Flow rate through pinhole: 3 SLM – Cell Pressure: 1 Torr | MCM OH yield (referenced to initial $[RO_2]$) assuming a reaction time of 1.9 ms, a temperature of 255 K and $[NO] = 1 \times 10^{14}$ molecule cm$^{-3}$ | Cell C, OH yield – Residence time: ~60 ms[c] – Typical NO flow used during fieldwork: 100 SCCM – Flow rate through pinhole: 3.5 SLM – Cell Pressure: 1.5 Torr | MCM OH yield (referenced to initial $[RO_2]$) assuming a reaction time of 70 ms, a temperature of 298 K and $[NO] = 9.5 \times 10^{14}$ molecule cm$^{-3}$ |
|---|---|---|---|---|---|---|---|
| Ethene | 10 | $0.057 \pm 0.033$ | | $0.463 \pm 0.030$ | 0.446 | – | |
| | 20 | $0.073 \pm 0.029$ | | – | | – | |
| | 30 | $0.098 \pm 0.025$ | | – | | – | |
| | 40 | $0.157 \pm 0.047$ | | – | | – | |
| | 50 | $0.172 \pm 0.057$ | 0.170 | – | | – | |
| | 100 | – | | – | | $0.947 \pm 0.073$ | 0.936 |
| Methanol | 50 | $0.756 \pm 0.273$ | 1.000 | – | | – | |
| Isoprene | 50 | $0.178 \pm 0.075$ | 0.175 | – | | $0.849 \pm 0.057$ | 0.871 |
| Propane | 50 | $0.000 \pm 0.053$ | 0.004 | $0.000 \pm 0.102$ | 0.004 | – | |
| Methane | 100 | – | | – | | $0.000 \pm 0.091$ | $4.8 \times 10^{-4}$ |
| Cyclohexane | 100 | – | | – | | $0.606 \pm 0.051$ | 0.575 |
| Toluene | 100 | – | | – | | $0.874 \pm 0.072$ | 0.900 |

[a] Determined by computational fluid dynamics, for further details refer to Creasey et al. (1997b). [b] Experiments during which the NO concentration was varied from 10–50 SCCM and compared to modelled OH yields (see Fig. 4) suggest that the NO that mixes into to the air flow is actually 5.5 times less than the NO that is injected. [c] Estimated from comparison of experimentally determined OH yield from ethane-derived $RO_2$ radicals and MCM-predicted yields.

was sufficient time for complete conversion of $RO_2$ to OH. The time-resolved flow tube experiments were not performed on a field instrument used for ambient $HO_2$ detection and so the purpose of these experiments, rather than gauge the level of interference suffered, was to experimentally determine the yield of OH from a range of $RO_2$ radicals in the presence of NO to compare to MCM recommendations. The time-resolved experiments enabled long reaction times to be reached, allowing the conversion of $RO_2$ to OH to proceed to completion, and providing a measure of the asymptotic yields of $HO_2$.

The time-resolved OH signals observed for a selection of $RO_2$ species tested are shown in Fig. 3, and Table 2 summarises the OH yields for all $RO_2$ investigated. In the absence of reagent, an OH signal was observable (upper panel, Fig. 3) which decayed at a rate of $\sim 25\,s^{-1}$. This loss can be attributed to reaction of OH with ozone that was present and diffusion of the radical out of the photolysis beam area. Upon addition of a reagent to the flow tube, OH was converted to $RO_2$ at $> 1000\,s^{-1}$. This rapid conversion ensured that the different $RO_2$ generated were present at the same concentration as each other (allowing relative yields to be determined) and that all the OH initially generated was consumed in the flow tube (given the residence time of 4 s) thus allowing a single exponential fit to be applied to the $RO_2$ signals displayed in the lower panel of Fig. 3. The slow decay ($\sim 5\,s^{-1}$) of the radical signal, displayed in the lower panel of Fig. 3, may be attributed primarily to diffusion of the radicals out of the photolysis beam area and, to a lesser extent (no greater than $1\,s^{-1}$), to radical–radical reaction.

As the initial OH concentration generated and subsequent $HO_2$ or $RO_2$ concentration generated within the flow tube were uncalibrated, the absolute OH yields within the FAGE expansion cell from the different $RO_2$ species were determined by comparing with the OH signal observed from $HO_2$ generated in the methanol experiments which has a 100 % yield. An exponential function of the form: OH signal $= y_0 + A \times \exp(-B \times$ probe delay time) was fitted to each OH temporal profile associated with the different $RO_2$ species investigated. To determine the relative yields of OH, the ratio of the $A$ factor for each fit relative to the $A$ factor determined for the methanol fit was calculated using Eq. (2):

$$\text{Relative OH yield} = A\ \text{factor}_{(\text{reagent})} : A\ \text{factor}_{(\text{methanol})}. \quad (2)$$

In agreement with Fuchs et al. (2011), a large OH yield from alkene-derived $RO_2$ radicals was observed (see Table 2) when NO was present in the FAGE cell. Smaller, but still significant, OH yields were also observed for $RO_2$ radicals derived from cyclohexane, *n* butane and *n* pentane (Table 2); the OH signal observed for propane-derived $RO_2$ radicals was negligible (upper limit of 4 %).

In several experiments, it was found that ethene-derived $RO_2$ radicals when compared to $HO_2$ from methanol had OH yields greater than one. The formation of $\beta$-hydroxy peroxy radicals is fast in the flow tube, and, if complete $RO_2$ titration to $HO_2$ and ultimately to OH was occurring in the FAGE cell then the ratio of the OH signals observed in the presence of ethene and methanol would be expected to equal one; a value greater than one suggests incomplete conversion of methanol to $HO_2$ in the flow tube. It was observed in

**Table 2.** OH yields in time-resolved experiments from peroxy radicals determined using Eqs. (2) and (3); the MCMv3.2 OH yield is provided in the final columns for comparison. The modelled OH yield was determined using Eq. (4) calculated after 9.8 ms integration time. The model was constrained with a [NO] = $1 \times 10^{14}$ molecule cm$^{-3}$ and a temperature = 298 K (fourth column) or [NO] = $1 \times 10^{14}$ molecule cm$^{-3}$ and a temperature = 255 K (final column).

| Source of peroxy radicals | OH yield (referenced to methanol) | OH Yield (referenced to ethene) | MCM OH yield (referenced to initial [$RO_2$]) at 298 K | MCM OH yield (referenced to initial [$RO_2$]) at 255 K |
|---|---|---|---|---|
| Methanol | $1.00 \pm 0.08$ | $0.85 \pm 0.09$ | 1.00 | – |
| Isoprene | $0.89 \pm 0.05$ | $0.92 \pm 0.04$ | 0.90 | – |
| Ethene | $1.06 \pm 0.04$ | $1.00 \pm 0.08$ | 0.99 | 0.90 |
| Cyclohexane | | $0.38 \pm 0.08$ | 0.74 | 0.36 |
| Propane | | $0.034 \pm 0.008$ | 0.01 | – |
| *n* Butane | | $0.18 \pm 0.01$ | 0.13 | 0.12 |
| *n* Pentane | | $0.48 \pm 0.01$ | 0.62 | 0.49 |

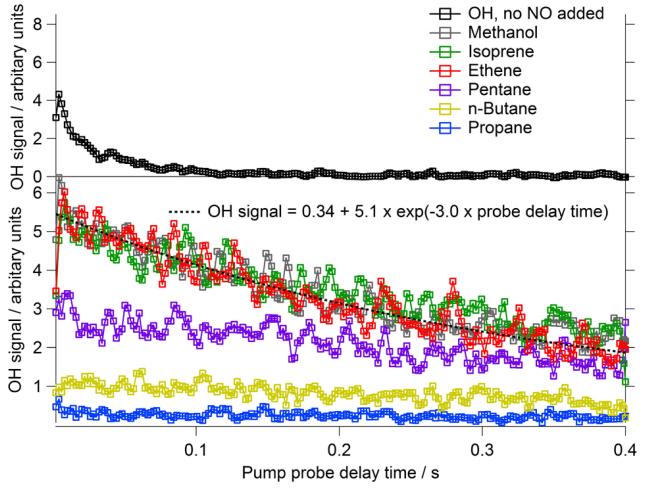


**Fig. 3.** (Upper panel) time evolution of OH formed in the flow tube by laser-photolysis of $O_3$ in humidified air in the absence of reagent with no NO added to the FAGE cell. The observed decay of $\sim 25\,s^{-1}$ may be attributed to reaction of OH with ozone and diffusion of the radical out of the photolysis beam area. (Lower panel) typical time-resolved experiments showing the OH signal from isoprene (green), ethene (red), methanol (grey), *n* pentane (purple), *n* butane-derived (mustard) and propane-derived (blue) peroxy radicals that was observed when 6 SCCM NO was added to the FAGE cell, and the relevant VOC reagent added to the flow tube to convert OH quantitatively to $RO_2$. The dashed line shows the fit to the OH signal from ethene-derived $RO_2$ radicals of the function: OH signal = $y_0 + A \times \exp(-B \times$ probe delay time). The signal decay ($\sim 5\,s^{-1}$) observed in the lower panel (i.e. the *B* parameter) may be attributed primarily to diffusion of the radicals out of the photolysis beam area and to a lesser extent ($\sim 1\,s^{-1}$) to radical-radical reaction. The relative yields were determined from the ratio of the *A* factors. See Table 2 for the yields determined.

experiments where the Pyrex bulb containing methanol was left for a full day before use to allow for mixing rather than just a couple of hours, that yields closer to one were obtained indicating that in several of the experiments there may have been insufficient methanol reaching the flow tube owing to extremely slow mixing of the gas bulb. To ensure that the results are not biased by a possible problem with methanol, column 2, Table 2 only includes relative OH yields calculated when the methanol bulb had been left for a day or longer. As this constraint limited the amount of data available, a third column which presents the OH yields referenced with respect to ethene (calculated using Eq. 3) is also provided:

$$\text{Relative OH yield} = A\ \text{factor}_{(\text{reagent})} : A\ \text{factor}_{(\text{ethene})}. \quad (3)$$

## 4 Discussion

### 4.1 Time-resolved experiments. Measured and modelled $HO_2$ yields following complete conversion of $RO_2$

Under conditions optimised for complete conversion of $RO_2$ radicals to OH in a FAGE cell with added NO (i.e. very long reaction times), the yield of $HO_2$ from a number of alkene-derived $RO_2$ species compares favourably to the MCMv3.2 predictions of the OH yield determined using Eq. (4) after a reaction time of 9.8 ms, as shown in Table 2. This suggests that the yield of $HO_2$ from other $RO_2$ species not measured here can be derived with some confidence from MCM predictions for this particular experimental set-up.

$$\text{MCM OH yield} = \frac{\text{modelled [OH] generated}}{\text{model initialised [RO}_2\text{]}}. \quad (4)$$

For greater than $C_3$ alkane-derived $RO_2$ species, the MCM also predicts a non-zero $HO_2$ yield. For these species, reaction with NO produces an alkoxy radical which can react with $O_2$ or isomerise forming a $\beta$-hydroxyalkylperoxy radical in the presence of $O_2$, which for the case of *n* butane-derived peroxy radical is:

$$C_4H_9O_2 + NO \rightarrow C_4H_9O + NO_2 \quad (R20)$$

$$C_4H_9O \xrightarrow{\text{isom.}} (HO)C_4H_8 \quad \text{(R21)}$$

$$(HO)C_4H_8 + O_2 \rightarrow (HO)C_4H_8O_2 \quad \text{(R22)}$$

The alkoxy radical, $C_4H_9O$, may also react with NO under FAGE conditions:

$$C_4H_9O + NO \rightarrow C_4H_9ONO \quad \text{(R23)}$$

As shown in Reactions (R8–R11) the $\beta$-hydroxyalkylperoxy radical can react further with NO and decompose rapidly in the presence of $O_2$ to form $HO_2$. However, as seen in Table 2, the MCM over-predicts the yield of $HO_2$ at 298 K from *n* pentane and cyclohexane-derived peroxy radicals, and under-predicts the OH yield from *n* butane-derived alkanes. The modelled to measured agreement for *n* pentane and cyclohexane-derived $RO_2$ radicals can be improved if the rate coefficient for isomerisation (Reaction R21) is reduced by assuming a lower temperature; it was found by varying the temperature in the model that 255 K provided the best agreement for all $RO_2$ species considered (Table 2). In the case of cyclohexane, the rate coefficient for isomerisation (taken from the MCMv3.2) decreases from $6.3 \times 10^4\,s^{-1}$ to $2.1 \times 10^3\,s^{-1}$ as the temperature was reduced from 298 K to 255 K. Stevens et al. (1994) report a temperature of 245 K within the Penn State FAGE instrument as an airstream enters the detection cell and accelerates to velocities of $> 300\,m\,s^{-1}$; at the laser detection axis the velocity is reduced to $\sim 50\,m\,s^{-1}$ and the air temperature increases to ambient levels once more. Similarly, measurements of rotational temperatures and computational fluid dynamic (CFD) calculations performed to determine the temperature and density profiles of an airstream within a Leeds FAGE detection cell, type A (Fig. 1a), suggest that air temperatures drop as low as 25 K in the first 2 cm in the detection cell beneath the pinhole as the airstream expands supersonically and reaches velocities of $750\,m\,s^{-1}$ before slowing and increasing back to ambient temperatures at the detection axis (Creasey et al., 1997b). Taking these temperature profiles into account, it is expected that the mean temperature experienced between pinhole and the detection axis will be below ambient and if this is the case the rate coefficient for isomerisation will slow considerably (Orlando et al., 2003). At lower temperatures the reaction between an alkoxy radical and NO (Reaction R19) can begin to compete with the isomerisation Reaction (R21) and can, as a result, lower the overall OH yield observed from these $RO_2$ radicals. This effect reduces the agreement between the experimental and modelled OH yield from *n* butane-derived $RO_2$ further suggesting that the rate coefficient for isomerisation of the $C_4H_9O$ alkoxy radical may actually be faster than assumed in the model. There is very little information on the temperature dependence associated with the rate of $\beta$-hydroxyalkoxy decomposition in the literature. A theoretical temperature dependence for the rate of decomposition of ethene-derived $\beta$-hydroxyalkoxy radical has been reported (Kukui and Le Bras, 2001):

$$k_{\text{decomp.}} = 1.1 \times 10^{13}[s^{-1}].e^{\frac{-41.84[\text{KJ mole}^{-1}]}{RT}}. \quad (5)$$

When this temperature dependence is included in model calculations, assuming a temperature of 255 K, the OH yield predicted is reduced by $\sim 10\,\%$ from calculations assuming a temperature of 298 K (Table 2) as the rate coefficient for decomposition decreases from $5.1 \times 10^5\,s^{-1}$ to $3.0 \times 10^4\,s^{-1}$. Although likely to be similar to that of the ethene-dervied alkoxy radical, no information on the temperature dependence of isoprene-derived alkoxy radical decomposition exists in the literature so the impact on the OH yield at reduced temperatures is not considered here.

### Magnitude of the interference for fieldwork instruments

For the three fieldwork FAGE cells tested (Fig. 1) which have different residence times and, hence reaction times for $RO_2$ conversion to OH, the yield of OH from the alkene-derived $RO_2$ radicals was variable. For cell A, CFD calculations have demonstrated that the air stream is significantly accelerated within the cell (and, in turn, is significantly cooled), owing to the supersonic expansion after the small diameter (1 mm) pinhole. Similar acceleration and cooling may be assumed for cell B as a 1 mm pinhole was again used. In cell C, air entered the FAGE cell through a 4 mm pinhole and so the same level of acceleration or cooling, as predicted in cell A, is not expected. For cell C, it may be expected that NO should mix reasonably well with the ambient air stream also. The best agreement between the MCM predictions and experimental results occurs if a contact time (and [NO]) of $\sim 0.9$ ms (and $1 \times 10^{14}$ molecule $cm^{-3}$), $\sim 1.9$ ms (and $1 \times 10^{14}$ molecule $cm^{-3}$) and $\sim 70$ ms (and $9.5 \times 10^{14}$ molecule $cm^{-3}$) is assumed for cell A, cell B and cell C (Fig. 1), respectively, at a temperature of 255 K for cells A and B and 298 K for cell C. For cell A, a residence time from pinhole to detection region of $< 1$ ms has been calculated using CFD (Creasey et al., 1997b) and compares favourably to the estimated contact time of 0.9 ms (estimated from the time at which the modelled yields best agree with the experimental relative yields, Table 1). As it is difficult to calculate the cell residence absolutely, due to the free-jet expansion that occurs, comparison of the yields with model predictions provides a means to gauge the time spent between the NO injection region and detection region experimentally. Uncertainty in the residence time may arise, however, if the NO injected into the cell does not fully mix with the sampled air stream or if the mean temperature of the airstream is not considered or known. Qualitatively, the extent of the interference suffered is directly proportional to residence time within the jet and inversely proportional to the mean temperature experienced by the jet (Eq. 6). At ambient temperatures, increasing the NO concentration will lead to an increase in the

interference; at reduced temperatures, however, the impact of NO becomes more complex: increasing the concentration of NO will increase the rates of Reactions (R3) and (R5) but also increases the rate of Reaction (R19). For alkoxy radicals which display a strong temperature dependence with respect to isomerisation, as is the case for the alkoxy radical derived from cyclohexane (CHEXO), increasing NO concentrations beyond a certain concentration may actually lead to a reduction in the level of interference observed as Reaction (R19) begins to compete effectively with Reaction (R21). Model simulations looking at the yield of OH from cyclohexane-derived $RO_2$ radicals at 255 K predict that at a residence time of 9.8 ms (time over which time-resolved experiments were run) the yield of OH will increase with increasing [NO] until a NO concentration of $1.2 \times 10^{14}$ molecule cm$^{-3}$ is reached and then the yield will begin to decrease as [NO] increases further. Note, if the residence time is increased, less NO is required to achieve the maximum yield and vice versa. Under the experimental conditions discussed in this paper the OH yield should have been directly proportional to [NO]:

$$\text{Interference } \alpha \frac{\text{Residence time} \times [\text{NO}]}{\text{Temperature}}. \quad (6)$$

Fuchs et al. (2011) observed a large under-prediction of the OH yield from cyclohexane-derived $RO_2$ radicals in the presence of NO and suggested that the model under-prediction for the yield of OH from this species may reflect a missing ring opening mechanism in the MCM which could promote further $HO_2$ formation. Fuchs et al. (2011) used MCMv3.1 which did not contain a ring opening mechanism to estimate the expected level of interference in the Julich FAGE system. An additional degradation pathway for CHEXO which includes a ring opening route, is included in MCMv3.2 leading to the yield of $HO_2$ (and ultimately OH, following further reaction) from cyclohexane-derived $RO_2$ radicals approximately doubling when switching from MCMv3.1 to MCMv3.2 chemistry.

### 4.2 Minimising the $RO_2$ interference further

As highlighted in Table 1, a decrease in the amount of NO injected into cell A reduces the OH yield from ethene-derived $RO_2$ radicals. Reducing the sensitivity of the instrument to the interference, however, leads to a concomitant reduction in $HO_2$ sensitivity. As only one NO molecule is required to titrate one $HO_2$ radical to OH, whilst two or more are required for $RO_2$ to OH titration, it is possible to begin to discriminate between $HO_2$ and $RO_2$ by reducing the amount of NO mixed into the jet as shown in Fig. 4. For cell A, at an NO concentration of $1 \times 10^{13}$ molecule cm$^{-3}$, approximately twenty $HO_2$ radicals titrate to OH for one $RO_2i$ radical conversion to OH; determined from the ratio "relative OH yield (propane) : relative OH yield (ethene)" with "relative OH yield" calculated using Eq. (1). At this NO concentration the 5 min limit of detection of the instrument for $HO_2$ will be $\sim 4 \times 10^6$ molecule cm$^{-3}$ and, although higher than detection limits from earlier campaigns (e.g. the $HO_2$ LOD during the SOAPEX campaign which took place in Cape Grim in Australia was $5.4 \times 10^5$ molecule cm$^{-3}$ for 2.5 min integration time) (Creasey et al., 2003), the instrument remains sufficiently sensitive for ambient $HO_2$ detection with minimal $RO_2$ interference ($\sim 5$ %). It should be noted that agreement between the MCMv3.2 model and observations can only be achieved if it is assumed that 5.5 times less NO is mixed fully into the air sample within the FAGE cell than is actually injected. Even when a reduced [NO] is assumed, the model predicted $HO_2 : RO_2$ ratio vs. [NO] is not wholly consistent with the ratio observed experimentally. As displayed in Fig. 4, the observed ratio increases slower than the model predicts as [NO] decreases (most apparent at the lowest [NO]) suggesting an enhanced $RO_2 \rightarrow$ OH conversion relative to $HO_2 \rightarrow$ OH conversion. This observation may indicate that $HO_2$ is preferentially lost in the cell compared to $RO_2$ radicals, potentially, by more efficient removal of $HO_2$ relative to $RO_2$ by $H_2O$ clusters (Creasey et al., 2001). This finding only serves to further highlight the need to experimentally determine the level of interference for each individual FAGE system and specific experimental conditions.

As demonstrated by Fig. 4, by varying the amount of NO injected it is possible to switch from conditions where certain $RO_2$ types are efficiently converted to OH (NO $> 5 \times 10^{13}$ molecule cm$^{-3}$) to conditions were the conversion is poor (NO $< 1 \times 10^{13}$ molecule cm$^{-3}$). With knowledge of the conversion efficiency of $RO_2$ and $HO_2$ at different NO concentrations, changing the NO flow during ambient measurements can selectively provide a measurement of the concentration of $RO_2i$ and $HO_2$ by simultaneously solving Eqs. (7) and (8):

$$\text{HO}_\text{x}\ \text{signal}_{\text{low [NO]}} = \text{C}_{\text{HO}_2,\ \text{low [NO]}} \times ([\text{HO}_2] + \alpha_{\text{low [NO]}}[\text{RO}_2i]) \quad (7)$$

$$\text{HO}_\text{x}\ \text{signal}_{\text{high [NO]}} = \text{C}_{\text{HO}_2,\text{high [NO]}} \times ([\text{HO}_2] + \alpha_{\text{high [NO]}}[\text{RO}_2i]), \quad (8)$$

where $HO_x$ signal is the fluorescence signal observed in cts s$^{-1}$ mW$^{-1}$, $C_{HO_2}$ is the sensitivity of the instrument to $HO_2$ (determined by calibration) at a particular NO flow in units of cm$^3$ molecule$^{-1}$ ct s$^{-1}$ mW$^{-1}$ and $\alpha$ is the mean fractional contribution of $RO_2i$ at a selected [NO].

During a recent field project, the Clean Air for London campaign (ClearfLo), this approach was adopted during ambient measurements. The NO concentration injected into a FAGE cell (cell type A) used during the campaign for sequential measurements of OH and $HO_2$ was varied between $\sim 1$ and $9 \times 10^{13}$ molecule cm$^{-3}$; a measurement of the total [$RO_2$] was determined simultaneously using the $RO_x$LIF cell C operating in $RO_x$ mode. The campaign average diurnal profile of $HO_2$, alkene/aromatic or long-chain alkane-derived $RO_2$ and short-chain alkane-derived $RO_2$ radicals selectively

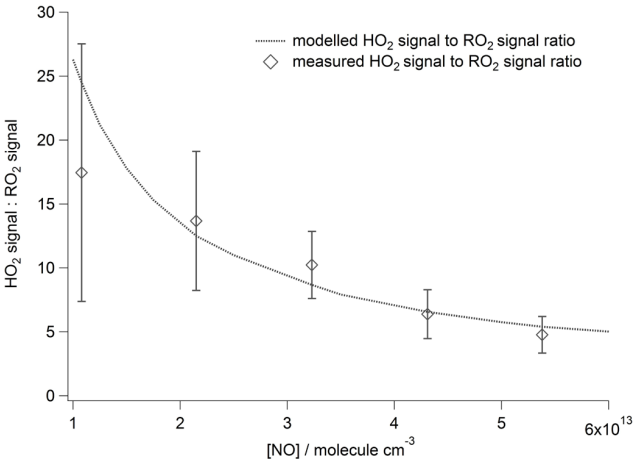


**Fig. 4.** Modelled (dashed line) and measured (open diamonds) ratio of the OH yield from $HO_{2\,signal} : RO_{2\,signal}$ as a function of NO concentration determined for cell A. For best agreement with model predictions, it has to be assumed that the NO concentration that mixes into the ambient air stream is 5.5 times lower than the amount actually injected. The error bars represent the fractional error associated with each measured ratio determined from the $1\sigma$ standard deviation of the experiments conducted.

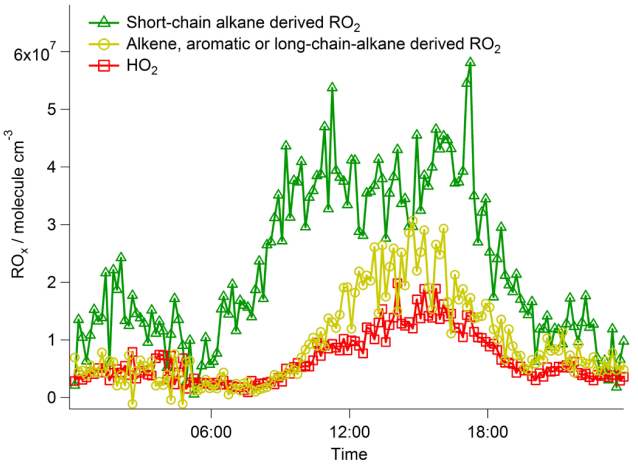


**Fig. 5.** Campaign averaged diurnal profiles of short-chain alkane $RO_2$ radicals (green), $HO_2$ (red) and alkene or aromatic or long-chain alkane-derived $RO_2$ radicals (mustard) from the ClearfLo project which took place in London (North Kensington) from the 21 July to 18 August 2012.

measured is provided in Fig. 5. The [$HO_2$] (red) and [$RO_2i$] (mustard) have been derived using Eqs. (7) and (8) (i.e. from $HO_2^*$ signal observed when using cell A at low and high NO flows; with the sensitivity to $HO_2$ and $RO_2i$ determined experimentally at the two NO flows used). The C1–C3 alkane-derived [$RO_2$] (green) was determined from cell C detection of total [$RO_x$] with the derived [$HO_2$] and [$RO_2i$] subtracted. In generating Fig. 5, it was assumed that all $RO_2i$ ($RO_2$ species which interfere) had the same conversion efficiency ($\alpha$) as ethene-derived $RO_2$. This assumption, whilst reasonable for other $RO_2$ radicals derived from other alkenes or aromatic VOC, may positively bias the [$RO_2i$] and negatively bias [$HO_2$] calculated if longer chain alkane-derived $RO_2$ ($\geq$ C4) which have a lower $\alpha$ were present at significant levels. Preliminary box modelling studies run for the ClearfLo project, which were constrained by the measurements of a wide range of VOCs of various classes, demonstrate that aromatic and alkene $RO_2$ species do dominate $RO_2i$, with $\geq$ C4 alkane-derived $RO_2$ species only contributing 7 % to all $RO_2i$ identified on average. For this particular environment at least (and likely applicable to many others), determining $HO_2$ and $RO_2i$ by the methodology discussed here may provide reasonable results.

An alternative approach to partial speciation of $RO_2$ radical classes would be to use two FAGE cells in which the $RO_2$ interference is minimised in the first (e.g. cell A, run at a low [NO]) and maximised in the second (e.g. cell C, $HO_x$ mode, run at a high [NO]).

### 4.3 Impact on previous field studies

The University of Leeds ground-based FAGE instrument has been operational since 1996 and has taken part in 17 campaigns with $HO_2$ measurements made during 13; see Table 3 for further details. In some of the earlier campaigns good conversion of $HO_2$ to OH was achieved as two independent cells were used, e.g. Smith et al. (2006), with the conditions of one cell optimised for $HO_2$ detection, and so a significant portion of $RO_2i$, if present, may also have been titrated to OH, constituting an interference. Many of the previous campaigns took place under relatively clean, unpolluted conditions, for example EASE-96 (Carslaw et al., 1999a), EASE-97 (Creasey et al., 2002; Carslaw et al., 2002), SOAPEX (Creasey et al., 2003; Sommariva et al., 2004), NAMBLEX (Sommariva et al., 2006), CHABLIS (Bloss et al., 2010), RHaMBLe (Whalley et al., 2010) where the concentrations of $RO_2i$ are likely low and methyl peroxy radicals, which do not give an interference (Ren et al., 2004), were expected to be the dominant $RO_2$ species; for example, during EASE-96 the model predicted that 92 % of peroxy radicals present were either $HO_2$ (53 %) or $CH_3O_2$ (39 %) during unpolluted conditions (Carslaw et al., 1999a). Similarly, for the SOS project (Vaughan et al., 2012), which took place in Cape Verde, models predicted that $\sim$ 90 % of peroxy radicals were either $HO_2$ or $CH_3O_2$. In general, models run for these campaigns tended to over-predict $HO_2$ despite additional $HO_2$ loss mechanisms such as reaction with halogen oxides and/or heterogeneous loss to aerosol surfaces in the model description. In contrast, under polluted, urban conditions (e.g. PUMA, Heard et al., 2004; TORCH-1, Emmerson et al., 2007) models either significantly under-predicted $HO_2$ observations (PUMA) (Emmerson et al., 2005) or

**Table 3.** Model: measured $HO_2$ ratio reported for the University of Leeds ground-based FAGE system during field campaigns where $HO_2$ measurements were made.

| Campaign | Model-measurement agreement for $HO_2$ | Cell-type | Reference |
|---|---|---|---|
| EASE-96 | Limited data, but tendency for model to overestimate $HO_2$ | A | Carslaw et al. (1999a) |
| AEROBIC | Modelled $HO_2$ was typically higher than observations, but observations showed a high degree of variability | A | Carslaw et al. (2001) |
| EASE-97 | Modelled : measured ratio of 3.6 | A | Carslaw et al. (2002) |
| SOAPEX | Modelled : measured ratio of 1.4 | A | Sommariva et al. (2004) |
| PUMA-summer | Modelled : measured ratio of 0.56 | A | Emmerson et al. (2005) |
| PUMA-winter | Modelled : measured ratio of 0.49 | A | Emmerson et al. (2005) |
| NAMBLEX | Good agreement within combined uncertainties | A | Sommariva et al. (2006) |
| TORCH | Good agreement within combined uncertainties; modelled : measured ratio of 1.07 | A | Emmerson et al. (2007) |
| CHABLIS | Modellled : measured ratio of 2 | A | Bloss et al. (2010) |
| RHaMBLe | Good agreement within combined uncertainties | A | Whalley et al. (2010) |
| OP3 | Modelled : measured ratio of 1.75 (standard chemistry model) | A | Whalley et al. (2011) |
| HCCT | Good agreement within combined uncertainties during the daytime | B | |
| ClearfLo | Modelling studies underway | A & C | |

were in relatively good agreement (TORCH-1) (Emmerson et al., 2007). If elevated concentrations of alkene-derived, aromatic-derived and higher alkane-derived $RO_2$ species were present, the true ambient $HO_2$ concentrations, as opposed to $HO_2^*$, were likely lower than reported. It is possible, although difficult to verify without observations of speciated $RO_2$, that the conclusions drawn from these observations, for example, that additional $HO_2$ sources in models are required to replicate observations, may be in error.

Under the operating conditions employed during the OP3 campaign, the instrument was relatively insensitive to detection of $RO_2$ species. The experiments presented here reveal a 17 % yield of OH due to the decomposition of ethene-derived $RO_2$ in the presence of NO in the FAGE detection cell under OP3 conditions. This provides an upper limit to the $HO_2$ yield from $RO_2$ species during OP3 as, under conditions in which the interference signal was maximised (Sect. 3.2), ethene-derived $RO_2$ species provided the largest $HO_2$ yield compared with other $RO_2$ species. Model simulations (Whalley et al., 2011) suggested that up to $2.1 \times 10^8$ molecule cm$^{-3}$ of potentially interfering $RO_2$ species were present at solar noon during OP3 (with isoprene-derived peroxy radicals contributing $\sim$60 % to this total), and thus up to $3.5 \times 10^7$ molecule cm$^{-3}$ of the $HO_2$ concentration may be attributed to these species ($\sim$10 % of the total $HO_2$ signal observed; Whalley et al., 2011). Model comparisons with the radical measurements made during the campaign demonstrated a large missing OH source and over-predicted the $HO_2$ observations. The small positive bias on the $HO_2$ observations, owing to the small yield of $HO_2$ from $RO_2$ species, only serves to reduce the modelled to measured agreement further. For the HCCT-2010 campaign, the potential impact of the interfering $RO_2$ species is greater (Table 1) owing to the smaller cell (with a longer inlet) and longer residence time employed. The campaign took place in a pine forest, close to the summit of Mount Schmücke in the Thüringer Wald mountain range in East Germany, during September and October 2010. VOC measurements were made downwind of the measurement site. Only low concentrations of isoprene (50 pptv) were detected, however, suggesting that the concentration of $RO_2i$ were also low.

## 5 Conclusions and further work

Recent studies conducted on a number of different fluorescence cells used in the FAGE instrument at Leeds have demonstrated that alkene- and aromatic-derived $RO_2$ species can yield appreciable quantities of OH upon addition of NO

in FAGE detection cells and, therefore, positively bias $HO_2$ observations if left uncorrected. Many FAGE groups now report $HO_2^*$ for comparison with atmospheric chemistry box models to include any interference from $RO_2i$. As demonstrated in this study, the magnitude of this interference is critically dependent on the cell design, quantity of NO used in the titration, the residence time and mean temperature of the air stream within the FAGE cell. The interference may be minimised by reducing NO concentrations and/or residence time, and although such a reduction will also reduce the sensitivity of the instrument to $HO_2$ (albeit to a lesser extent than the reduction in the sensitivity to $RO_2$ radicals) it will still be possible to detect ambient levels $HO_2$ using FAGE.

In laboratory, laser-flash photolysis experiments, under conditions optimised for complete conversion of $RO_2$ radicals to OH in a FAGE cell, the yield of $HO_2$ from a number of alkene-derived $RO_2$ species could be measured, and compared favourably with MCMv3.2 predictions. This suggests that the yield of $HO_2$ from other alkene-derived or aromatic-derived $RO_2$ species not tested here, but which are expected to exhibit high yields, could be determined from MCM predictions. The ability to discriminate between $HO_2$ and $RO_2i$ radicals, as illustrated for the ClearfLo project, is not only of great value for field measurements (and subsequent model comparisons), but such instrumentation may be used to selectively determine the yield of $HO_2$ in laboratory experiments under conditions where $RO_2$ radicals may also be present. Important applications, for example, would be the experimental verification of a significant prompt $HO_2$ yield from OH initialised isoprene oxidation, as proposed by Peeters et al. (2009) or prompt $HO_2$ yields from OH initialised oxidation of aromatics (Nehr et al., 2012).

This study demonstrates that some of the previous $HO_2$ measurements that depend upon chemical titration to OH by NO may suffer an interference due to partial detection of $RO_2$ radicals. Under conditions where there are significant alkene, aromatic or long-chain alkanes present, the $HO_2^*$ concentration which was measured will have been higher than the $HO_2$ concentration that was actually present. Models have overestimated $HO_2$ concentrations under such conditions, and this over-estimation would only increase if the observations of $HO_2$ were corrected for the interference suggesting there is a major gap in our understanding of the chemistry controlling these radicals.

*Acknowledgements.* We would like to thank the National Centre for Atmospheric Science (NCAS) for financial support and EUROCHAMP is acknowledged for PWS.

Edited by: A. Hofzumahaus

## References

Atkinson, R., Baulch, D. L., Cox, R. A., Hampson, R. F., Kerr, J. A., Rossi, M. J., and Troe, J.: Evaluated kinetic, photochemical and heterogeneous data for atmospheric chemistry .5. IUPAC Subcommittee on Gas Kinetic Data Evaluation for Atmospheric Chemistry, J. Phys. Chem. Ref. Data, 26, 521–1011, 1997.

Atkinson, R., Baulch, D. L., Cox, R. A., Crowley, J. N., Hampson, R. F., Hynes, R. G., Jenkin, M. E., Rossi, M. J., and Troe, J.: Evaluated kinetic and photochemical data for atmospheric chemistry: Volume I – gas phase reactions of $O_x$, $HO_x$, $NO_x$ and $SO_x$ species, Atmos. Chem. Phys., 4, 1461–1738, doi:10.5194/acp-4-1461-2004, 2004.

Bloss, C., Wagner, V., Jenkin, M. E., Volkamer, R., Bloss, W. J., Lee, J. D., Heard, D. E., Wirtz, K., Martin-Reviejo, M., Rea, G., Wenger, J. C., and Pilling, M. J.: Development of a detailed chemical mechanism (MCMv3.1) for the atmospheric oxidation of aromatic hydrocarbons, Atmos. Chem. Phys., 5, 641–664, doi:10.5194/acp-5-641-2005, 2005.

Bloss, W. J., Camredon, M., Lee, J. D., Heard, D. E., Plane, J. M. C., Saiz-Lopez, A., Bauguitte, S. J.-B., Salmon, R. A., and Jones, A. E.: Coupling of $HO_x$, $NO_x$ and halogen chemistry in the antarctic boundary layer, Atmos. Chem. Phys., 10, 10187–10209, doi:10.5194/acp-10-10187-2010, 2010.

Carslaw, N., Creasey, D. J., Heard, D. E., Lewis, A. C., McQuaid, J. B., Pilling, M. J., Monks, P. S., Bandy, B. J., and Penkett, S. A.: Modeling OH, $HO_2$, and $RO_2$ radicals in the marine boundary layer – 1. Model construction and comparison with field measurements, J. Geophys. Res.-Atmos., 104, 30241–30255, doi:10.1029/1999jd900783, 1999a.

Carslaw, N., Jacobs, P. J., and Pilling, M. J.: Modeling OH, $HO_2$, and $RO_2$ radicals in the marine boundary layer 2. Mechanism reduction and uncertainty analysis, J. Geophys. Res.-Atmos., 104, 30257–30273, doi:10.1029/1999jd900782, 1999b.

Carslaw, N., Creasey, D. J., Harrison, D., Heard, D. E., Hunter, M. C., Jacobs, P. J., Jenkin, M. E., Lee, J. D., Lewis, A. C., Pilling, M. J., Saunders, S. M., and Seakins, P. W.: OH and $HO_2$ radical chemistry in a forested region of north-western Greece, Atmos. Environ., 35, 4725–4737, doi:10.1016/S1352-2310(01)00089-9, 2001.

Carslaw, N., Creasey, D. J., Heard, D. E., Jacobs, P. J., Lee, J. D., Lewis, A. C., McQuaid, J. B., Pilling, M. J., Bauguitte, S., Penkett, S. A., Monks, P. S., and Salisbury, G.: Eastern Atlantic Spring Experiment 1997 (EASE97) – 2. Comparisons of model concentrations of OH, $HO_2$, and $RO_2$ with measurements, J. Geophys. Res.-Atmos., 107, ACH5.1–ACH5.16, doi:10.1029/2001jd001568, 2002.

Cleary, P. A., Romero, M. T. B., Blitz, M. A., Heard, D. E., Pilling, M. J., Seakins, P. W., and Wang, L.: Determination of the temperature and pressure dependence of the reaction $OH+C_2H_4$ from 200–400 K using experimental and master equation analyses, Phys. Chem. Chem. Phys., 8, 5633–5642, doi:10.1039/B612127f, 2006.

Commane, R., Floquet, C. F. A., Ingham, T., Stone, D., Evans, M. J., and Heard, D. E.: Observations of OH and $HO_2$ radicals over West Africa, Atmos. Chem. Phys., 10, 8783–8801, doi:10.5194/acp-10-8783-2010, 2010.

Creasey, D. J., HalfordMaw, P. A., Heard, D. E., Pilling, M. J., and Whitaker, B. J.: Implementation and initial deployment of a field instrument for measurement of OH and $HO_2$ in the tropo-

sphere by laser-induced fluorescence, J. Chem. Soc. Faraday T., 93, 2907–2913, doi:10.1039/A701469d, 1997a.

Creasey, D. J., Heard, D. E., Pilling, M. J., Whitaker, B. J., Berzins, M., and Fairlie, R.: Visualisation of a supersonic free-jet expansion using laser-induced fluorescence spectroscopy: Application to the measurement of rate constants at ultralow temperatures, Appl. Phys. B-Lasers O, 65, 375–391, doi:10.1007/s003400050285, 1997b.

Creasey, D. J., Heard, D. E., and Lee, J. D.: OH and $HO_2$ measurements in a forested region of north-western Greece, Atmos. Environ., 35, 4713–4724, doi:10.1016/S1352-2310(01)00090-5, 2001.

Creasey, D. J., Heard, D. E., and Lee, J. D.: Eastern Atlantic Spring Experiment 1997 (EASE97) 1. Measurements of OH and $HO_2$ concentrations at Mace Head, Ireland, J. Geophys. Res.-Atmos., 107, 4091, doi:10.1029/2001jd000892, 2002.

Creasey, D. J., Evans, G. E., Heard, D. E., and Lee, J. D.: Measurements of OH and $HO_2$ concentrations in the Southern Ocean marine boundary layer, J. Geophys. Res.-Atmos., 108, 4475, doi:10.1029/2002jd003206, 2003.

Davis, D. D., Rodgers, M. O., Fischer, S. D., and Asai, K.: An experimental assessment of the $O_3/H_2O$ interference problem in the detection of natural levels of OH via laser induced fluorescence, Geophys. Res. Lett., 8, 69–72, doi:10.1029/GL008i001p00069, 1981.

Emmerson, K. M., Carslaw, N., Carpenter, L. J., Heard, D. E., Lee, J. D., and Pilling, M. J.: Urban Atmospheric Chemistry During the PUMA Campaign 1: Comparison of Modelled OH and $HO_2$ Concentrations with Measurements, J. Atmos. Chem., 52, 143–164, 2005.

Emmerson, K. M., Carslaw, N., Carslaw, D. C., Lee, J. D., McFiggans, G., Bloss, W. J., Gravestock, T., Heard, D. E., Hopkins, J., Ingham, T., Pilling, M. J., Smith, S. C., Jacob, M., and Monks, P. S.: Free radical modelling studies during the UK TORCH Campaign in Summer 2003, Atmos. Chem. Phys., 7, 167–181, doi:10.5194/acp-7-167-2007, 2007.

Faloona, I., Tan, D., Brune, W., Hurst, J., Barket, D., Couch, T. L., Shepson, P., Apel, E., Riemer, D., Thornberry, T., Carroll, M. A., Sillman, S., Keeler, G. J., Sagady, J., Hooper, D., and Paterson, K.: Nighttime observations of anomalously high levels of hydroxyl radicals above a deciduous forest canopy, J. Geophys. Res.-Atmos., 106, 24315–24333, doi:10.1029/2000jd900691, 2001.

Fuchs, H., Holland, F., and Hofzumahaus, A.: Measurement of tropospheric $RO_2$ and $HO_2$ radicals by a laser-induced fluorescence instrument, Rev. Sci. Instrum., 79, 084104, doi:10.1063/1.2968712, 2008.

Fuchs, H., Bohn, B., Hofzumahaus, A., Holland, F., Lu, K. D., Nehr, S., Rohrer, F., and Wahner, A.: Detection of $HO_2$ by laser-induced fluorescence: calibration and interferences from $RO_2$ radicals, Atmos. Meas. Tech., 4, 1209–1225, doi:10.5194/amt-4-1209-2011, 2011.

Fuchs, H., Dorn, H.-P., Bachner, M., Bohn, B., Brauers, T., Gomm, S., Hofzumahaus, A., Holland, F., Nehr, S., Rohrer, F., Tillmann, R., and Wahner, A.: Comparison of OH concentration measurements by DOAS and LIF during SAPHIR chamber experiments at high OH reactivity and low NO concentration, Atmos. Meas. Tech., 5, 1611–1626, doi:10.5194/amt-5-1611-2012, 2012.

Fuchs, H., Hofzumahaus, A., Rohrer, F., Bohn, B., Brauers, T., Dorn, H. P., Haseler, R., Holland, F., Kaminski, M., Li, X., Lu, K., Nehr, S., Tillmann, R., Wegener, R., and Wahner, A.: Experimental evidence for efficient hydroxyl radical regeneration in isoprene oxidation, Nat. Geosci., online first, doi:10.1038/NGEO1964, 2013.

Hanisco, T. F., Smith, J. B., Stimpfle, R. M., Wilmouth, D. M., Anderson, J. G., Richard, E. C., and Bui, T. P.: In situ observations of $HO_2$ and OH obtained on the NASA ER-2 in the high-ClO conditions of the 1999/2000 Arctic polar vortex, J. Geophys. Res.-Atmos., 107, 8283, doi:10.1029/2001jd001024, 2002.

Hard, T. M., Obrien, R. J., Cook, T. B., and Tsongas, G. A.: Interference Suppression in OH Fluorescence Detection, Appl. Optics, 18, 3216–3217, doi:10.1364/Ao.18.003216, 1979.

Hard, T. M., Obrien, R. J., Chan, C. Y., and Mehrabzadeh, A. A.: Tropospheric Free-Radical Determination by Fage, Environ. Sci. Technol., 18, 768–777, doi:10.1021/Es00128a009, 1984.

Heard, D. E. and Pilling, M. J.: Measurement of OH and $HO_2$ in the troposphere, Chem. Rev., 103, 5163–5198, doi:10.1021/Cr020522s, 2003.

Heard, D. E., Carpenter, L. J., Creasey, D. J., Hopkins, J. R., Lee, J. D., Lewis, A. C., Pilling, M. J., Seakins, P. W., Carslaw, N., and Emmerson, K. M.: High levels of the hydroxyl radical in the winter urban troposphere, Geophys. Res. Lett., 31, L18112, doi:10.1029/2004gl020544, 2004.

Heicklen, J.: The Decomposition of Alkyl Nitrites and the Reactions of Alkoxyl Radicals, in: Advances in Photochemistry, John Wiley & Sons, Inc., 177–272, 2007.

Hewitt, C. N., Lee, J. D., MacKenzie, A. R., Barkley, M. P., Carslaw, N., Carver, G. D., Chappell, N. A., Coe, H., Collier, C., Commane, R., Davies, F., Davison, B., DiCarlo, P., Di Marco, C. F., Dorsey, J. R., Edwards, P. M., Evans, M. J., Fowler, D., Furneaux, K. L., Gallagher, M., Guenther, A., Heard, D. E., Helfter, C., Hopkins, J., Ingham, T., Irwin, M., Jones, C., Karunaharan, A., Langford, B., Lewis, A. C., Lim, S. F., MacDonald, S. M., Mahajan, A. S., Malpass, S., McFiggans, G., Mills, G., Misztal, P., Moller, S., Monks, P. S., Nemitz, E., Nicolas-Perea, V., Oetjen, H., Oram, D. E., Palmer, P. I., Phillips, G. J., Pike, R., Plane, J. M. C., Pugh, T., Pyle, J. A., Reeves, C. E., Robinson, N. H., Stewart, D., Stone, D., Whalley, L. K., and Yin, X.: Overview: oxidant and particle photochemical processes above a south-east Asian tropical rainforest (the OP3 project): introduction, rationale, location characteristics and tools, Atmos. Chem. Phys., 10, 169–199, doi:10.5194/acp-10-169-2010, 2010.

Hofzumahaus, A., Aschmutat, U., Hessling, M., Holland, F., and Ehhalt, D. H.: The measurement of tropospheric OH radicals by laser-induced fluorescence spectroscopy during the POPCORN field campaign, Geophys. Res. Lett., 23, 2541–2544, doi:10.1029/96gl02205, 1996.

Holland, F., Hofzumahaus, A., Schafer, R., Kraus, A., and Patz, H. W.: Measurements of OH and $HO_2$ radical concentrations and photolysis frequencies during BERLIOZ, J. Geophys. Res.-Atmos., 108, 8246, doi:10.1029/2001jd001393, 2003.

Ianni, J. C.: available at: http://www.kintecus.com (last access: 5 December 2013), Windows version 2.80 Edn., 2002.

Jenkin, M. E., Saunders, S. M., and Pilling, M. J.: The tropospheric degradation of volatile organic compounds: A protocol for mechanism development, Atmos. Environ., 31, 81–104, doi:10.1016/S1352-2310(96)00105-7, 1997.

Jenkin, M. E., Saunders, S. M., Wagner, V., and Pilling, M. J.: Protocol for the development of the Master Chemical Mechanism, MCM v3 (Part B): tropospheric degradation of aromatic volatile organic compounds, Atmos. Chem. Phys., 3, 181–193, doi:10.5194/acp-3-181-2003, 2003.

Kanaya, Y., Sadanaga, Y., Matsumoto, J., Sharma, U. K., Hirokawa, J., Kajii, Y., and Akimoto, H.: Nighttime observation of the $HO_2$ radical by an LIF instrument at Oki island, Japan, and its possible origins, Geophys. Res. Lett., 26, 2179–2182, doi:10.1029/1999gl900475, 1999.

Kukui, A. and Le Bras, G.: Theoretical study of the thermal decomposition of several beta-chloroalkoxy radicals, Phys. Chem. Chem. Phys., 3, 175–178, doi:10.1039/B007644i, 2001.

Lu, K. D., Rohrer, F., Holland, F., Fuchs, H., Bohn, B., Brauers, T., Chang, C. C., Häseler, R., Hu, M., Kita, K., Kondo, Y., Li, X., Lou, S. R., Nehr, S., Shao, M., Zeng, L. M., Wahner, A., Zhang, Y. H., and Hofzumahaus, A.: Observation and modelling of OH and $HO_2$ concentrations in the Pearl River Delta 2006: a missing OH source in a VOC rich atmosphere, Atmos. Chem. Phys., 12, 1541–1569, doi:10.5194/acp-12-1541-2012, 2012.

Mao, J., Ren, X., Zhang, L., Van Duin, D. M., Cohen, R. C., Park, J.-H., Goldstein, A. H., Paulot, F., Beaver, M. R., Crounse, J. D., Wennberg, P. O., DiGangi, J. P., Henry, S. B., Keutsch, F. N., Park, C., Schade, G. W., Wolfe, G. M., Thornton, J. A., and Brune, W. H.: Insights into hydroxyl measurements and atmospheric oxidation in a California forest, Atmos. Chem. Phys., 12, 8009–8020, doi:10.5194/acp-12-8009-2012, 2012.

Mather, J. H., Stevens, P. S., and Brune, W. H.: OH and $HO_2$ measurements using laser-induced fluorescence, J Geophys Res-Atmos, 102, 6427–6436, doi:10.1029/96jd01702, 1997.

Nehr, S., Bohn, B., and Wahner, A.: Prompt $HO_2$ Formation Following the Reaction of OH with Aromatic Compounds under Atmospheric Conditions, J. Phys. Chem. A, 116, 6015–6026, doi:10.1021/Jp210946y, 2012.

Orlando, J. J., Tyndall, G. S., and Wallington, T. J.: The atmospheric chemistry of alkoxy radicals, Chem. Rev., 103, 4657–4689, doi:10.1021/Cr020527p, 2003.

Ortgies, G., Gericke, K. H., and Comes, F. J.: Is UV Laser-Induced Fluorescence a method to monitor tropospheric OH?, Geophys. Res. Lett., 7, 905–908, doi:10.1029/Gl007i011p00905, 1980.

Peeters, J., Nguyen, T. L., and Vereecken, L.: $HO_x$ radical regeneration in the oxidation of isoprene, Phys. Chem. Chem. Phys., 11, 5935–5939, 2009.

Ren, X. R., Harder, H., Martinez, M., Faloona, I. C., Tan, D., Lesher, R. L., Di Carlo, P., Simpas, J. B., and Brune, W. H.: Interference testing for atmospheric $HO_x$ measurements by laser-induced fluorescence, J. Atmos. Chem., 47, 169–190, doi:10.1023/B:Joch.0000021037.46866.81, 2004.

Sadanaga, Y., Yoshino, A., Watanabe, K., Yoshioka, A., Wakazono, Y., Kanaya, Y., and Kajii, Y.: Development of a measurement system of OH reactivity in the atmosphere using a laser-induced pupm and probe technique, Rev. Sci. Instrum., 75, 2648–2655, 2004.

Saunders, S. M., Jenkin, M. E., Derwent, R. G., and Pilling, M. J.: Protocol for the development of the Master Chemical Mechanism, MCM v3 (Part A): tropospheric degradation of non-aromatic volatile organic compounds, Atmos. Chem. Phys., 3, 161–180, doi:10.5194/acp-3-161-2003, 2003.

Shirinzadeh, B., Wang, C. C., and Deng, D. Q.: Pressure dependence of ozone interference in the laser fluorescence measurements of OH in the atmosphere, Appl. Optics, 26, 12102–2105, 1987.

Smith, S. C., Lee, J. D., Bloss, W. J., Johnson, G. P., Ingham, T., and Heard, D. E.: Concentrations of OH and $HO_2$ radicals during NAMBLEX: measurements and steady state analysis, Atmos. Chem. Phys., 6, 1435–1453, doi:10.5194/acp-6-1435-2006, 2006.

Sommariva, R., Haggerstone, A.-L., Carpenter, L. J., Carslaw, N., Creasey, D. J., Heard, D. E., Lee, J. D., Lewis, A. C., Pilling, M. J., and Zádor, J.: OH and $HO_2$ chemistry in clean marine air during SOAPEX-2, Atmos. Chem. Phys., 4, 839–856, doi:10.5194/acp-4-839-2004, 2004.

Sommariva, R., Bloss, W. J., Brough, N., Carslaw, N., Flynn, M., Haggerstone, A.-L., Heard, D. E., Hopkins, J. R., Lee, J. D., Lewis, A. C., McFiggans, G., Monks, P. S., Penkett, S. A., Pilling, M. J., Plane, J. M. C., Read, K. A., Saiz-Lopez, A., Rickard, A. R., and Williams, P. I.: OH and $HO_2$ chemistry during NAMBLEX: roles of oxygenates, halogen oxides and heterogeneous uptake, Atmos. Chem. Phys., 6, 1135–1153, doi:10.5194/acp-6-1135-2006, 2006.

Stevens, P. S., Mather, J. H., and Brune, W. H.: Measurement of Tropospheric OH and $HO_2$ by Laser-Induced Fluorescence at Low-Pressure, J. Geophys. Res.-Atmos., 99, 3543–3557, doi:10.1029/93jd03342, 1994.

Stone, D., Whalley, L. K., and Heard, D. E.: Tropospheric OH and $HO_2$ radicals: field measurements and model comparisons, Chem. Soc. Rev., 41, 6348–6404, doi:10.1039/C2cs35140d, 2012.

Vaughan, S., Ingham, T., Whalley, L. K., Stone, D., Evans, M. J., Read, K. A., Lee, J. D., Moller, S. J., Carpenter, L. J., Lewis, A. C., Fleming, Z. L., and Heard, D. E.: Seasonal observations of OH and $HO_2$ in the remote tropical marine boundary layer, Atmos. Chem. Phys., 12, 2149–2172, doi:10.5194/acp-12-2149-2012, 2012.

Whalley, L. K., Furneaux, K. L., Goddard, A., Lee, J. D., Mahajan, A., Oetjen, H., Read, K. A., Kaaden, N., Carpenter, L. J., Lewis, A. C., Plane, J. M. C., Saltzman, E. S., Wiedensohler, A., and Heard, D. E.: The chemistry of OH and $HO_2$ radicals in the boundary layer over the tropical Atlantic Ocean, Atmos. Chem. Phys., 10, 1555–1576, doi:10.5194/acp-10-1555-2010, 2010.

Whalley, L. K., Edwards, P. M., Furneaux, K. L., Goddard, A., Ingham, T., Evans, M. J., Stone, D., Hopkins, J. R., Jones, C. E., Karunaharan, A., Lee, J. D., Lewis, A. C., Monks, P. S., Moller, S. J., and Heard, D. E.: Quantifying the magnitude of a missing hydroxyl radical source in a tropical rainforest, Atmos. Chem. Phys., 11, 7223–7233, doi:10.5194/acp-11-7223-2011, 2011.